ELSEVIER

Journal of Nuclear Materials 251 (1997) 276–283

journal of nuclear materials

Strains and stresses in ceramics by defect accumulation

P. Jung *, Z. Zhu, J. Chen

Institut für Festkörperforschung, Association EURATOM-KFA, Forschungszentrum Jülich, D-52425 Julich, Germany

Abstract

Measurements of uniaxial strains introduced in Al_2O_3, MgO, $AlMg_2O_4$, AlN, Si_3N_4 and SiC by light ion irradiation are compared to relative volume changes from neutron irradiation. The results are discussed in terms of a rate theoretical model of point defect retention which includes spontaneous recombination. Strains from defect accumulation were derived with even higher precision from the bending of inhomogenously irradiated or implanted thin specimens. Stress distribution in this case is calculated by the finite element method and limitations of analytical stress calculations are given. © 1997 Elsevier Science B.V.

1. Introduction

Ceramic materials are considered for application in future fusion reactors for various purposes, e.g., armor of first wall (SiC), structural material (SiC/SiC), insulators and HF-windows (Al_2O_3, etc.). Due to the low ductility of most ceramics, already small irradiation induced strains and stresses can cause failure [1]. The present work gives in Section 2 dimensional changes of various ceramic materials derived from uniaxial length measurements under proton irradiation. In Section 3 these measurements are interpreted by a model of defect accumulation and saturation. If irradiation is not homogeneous throughout the material internal stress are produced, mainly at the interface between irradiated layer and unirradiated bulk. This is described in Section 4 and applied to experimental results in Section 5.

2. Strains by defect production

Ceramic ribbons of 240 to 365 μm thickness were irradiated with protons in the 10 MeV range at the Jülich-Compact-Cyclotron from 220 to 505°C, with the present communication emphasizing the lower end of this temperatures range. 10 MeV protons have ranges in the order of 500 μm in the present materials. This means that damage is fairly homogeneous and no implantation occurs. Suppliers and specimen parameters are summarized in Table 1. Tensile stresses from 20 to 100 MPa were applied to improve the precision of uniaxial length measurement and to study possible effects of stress (creep). With the exception of MgO and vitreous SiO_2 (see Refs. [2,3]) no effect of stress on straining was observed.

The symbols in Fig. 1 indicate relative volume changes derived from uniaxial strains ($\Delta V/V = 3\epsilon$) of poly- and single crystalline Al_2O_3, induced by proton irradiation at temperatures around 230°C. The data are compared to volume changes from neutron irradiation and to model calculations given in the next chapter. For results on polycrystalline Al_2O_3 at higher temperatures see Refs. [2,11]. For comparison to the neutron irradiations, displacement per atoms (dpa) were used as dose unit. Displacement cross sections for protons and neutrons calculated according to the NRT model are included in Table 1 [2].

Figs. 2 and 3 compare relative volume changes of AlN and Si_3N_4 derived from uniaxial strain measurements under proton irradiation to neutron data. Only for AlN one data point at lower temperatures is available from neutron irradiation. In Fig. 4 relative volume changes of SiC derived from strain measurements at 265 and 505°C are compared to neutron data from 200 to 500°C. Results for

* Corresponding author. Tel.: +49-2461 614 036; fax: +49-2461 612 410; e-mail: p.jung@fz-juelich.de.

PII S0022-3115(97)00249-3

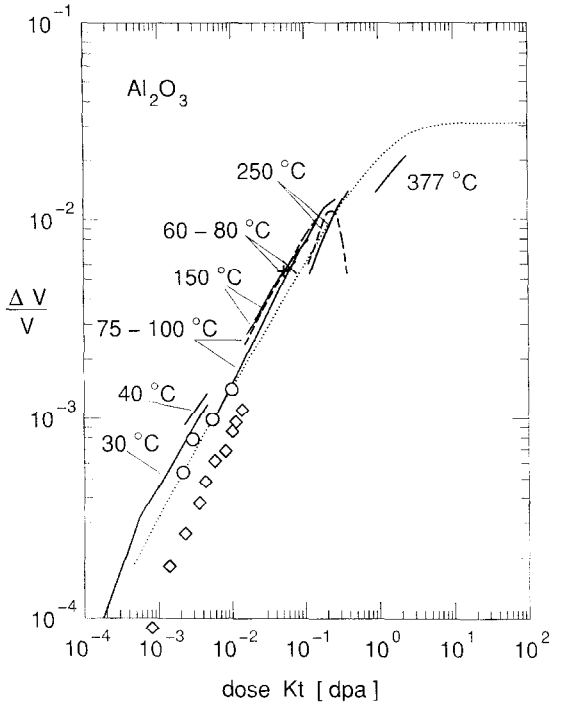

Fig. 1. Relative volume change of polycrystalline Al_2O_3 derived from uniaxial strains under proton irradiation at 235°C with tensile stress of 20 and 40 MPa (○) and of single crystals at 220°C and 40 MPa (◇). Included are results from neutron irradiations at 30°C [4], ≤ 40°C [5], 75–100°C [6], 150°C [7], 60–80°C [8], 250°C [9] and 377°C [10]. Dashed lines and crosses give lattice parameter measurements. The dotted line represents the calculations by the present model.

MgO and $AlMg_2O_4$ were published previously [3]. For these materials the fitting parameters to the model described in Section 3 are given in Table 1.

3. Model of defect retention

Recently a set of coupled rate equations for atomic concentrations of interstitials (c_i), vacancies (c_v) and loops radii (R_l) was solved under the assumption of immobile vacancies (diffusion coefficient $D_v \approx 0$), which is supposed to be representative for refractory metals and ceramics in the intermediate temperature range, cf. Refs. [2,3]. In contrast to previous treatments [18,19], the present model includes a volume for spontaneous recombination of isolated interstitials and vacancies [2,3], i.e., recombination of defects produced close to their already existing counterparts without thermal activation. It does not include spontaneous recombination of vacancies with interstitial loops and also no spontaneous formation and growth of defect clusters by stochastic agglomeration. For $D_i \gg D_v$ the interstitial concentration is low and quasi-stationary, i.e., $dc_i/dt \approx 0$ and thus the set of rate equations simplifies to

$$c_i = \frac{K(1 - v_r c_v)}{(Kv_r + q(D_i + D_v)c_v + Z_i D_i(\rho_d + \rho_l)}, \quad (1)$$

$$\frac{dc_v}{dt} \approx \frac{KZ_i D_i(1 - v_r c_v)(\rho_d + \rho_l)}{q(D_i + D_v)c_v + Kv_r + Z_i D_i(\rho_d + \rho_l)}, \quad (2)$$

$$\frac{dR_l}{dt} \approx \frac{dc_v/dt}{b(\rho_d + \rho_l)}, \quad (3)$$

with K (s^{-1}) the atomic displacement rate, v_r [1] the recombination volume in units of atomic volumes Ω (m^3), D_i and D_v (m^2/s) the diffusion coefficients, Z_i and Z_v [1] the bias factors, b (m) the Burger's vector and ρ_d (m^{-2}) the dislocation line density. The line density of loops is given by $\rho_l = 2\pi N_l R_l$, with N_l (m^{-3}) the loop density. The recombination strength q is given by $q = 4\pi R_0/\Omega$, with the recombination radius R_0. The relative volume changes are related to the concentration of retained vacancies by

$$\Delta V/V = v_F c_v, \quad (4)$$

where v_F is the relative volume change per Frenkel pair

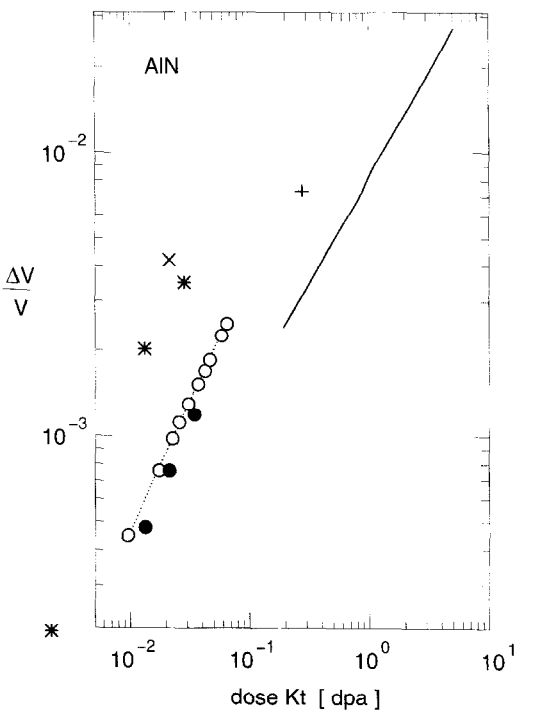

Fig. 2. Relative volume change from strains of AlN under proton irradiation at 230°C (○) and 420°C (●) at tensile stresses of 40 MPa. Included are results from neutron irradiation at 100°C (×), 470°C (+) [12], 400–550°C (solid line) [13] and < 600°C (*253) [14]. The latter data are from lattice parameter measurements.

Table 1
Displacement cross sections σ_d and fitting parameters for measurement at temperatures around 230°C

Material	Density (g/cm^3)	σ_d ($10-26\ m^2$)		Dose exponent (dose range (dpa))	$v_F^3 \cdot N_I/q^2$ (10^{-16} m)	Saturation $\Delta V/V$ (%)
		protons	neutrons			
Al_2O_3-p[a]	3.9	11	3.85	0.56 (0.002–0.01)	3.6	3.1
Al_2O_3-x[b]	3.96	11	3.85	0.93 (< 0.007) 0.73 (> 0.01)	–	–
MgO-x[c]	3.68	5.2	2.5	0.69 (0.0004–0.006) 0.78 (0.0005–0.006) 0.66 (0.0004–0.001)	5.4	3.1
$AlMg_2O_4$[d]	3.61	5.2	2.5	0.6 (0.001–0.002)	–	0.1[i]
AlN[e]	3.26	11	3.85	0.68 (0.001–0.01)	5.2	–[j]
Si_3N_4[f]	3.20	16	4.1	0.6 (0.001–0.02)	2.7	–[k]
SiC-HD[g]	3.2	16.5	7.3	0.78 (< 0.011)	–	2.8
SiC/C[h]	2.65	15.5	7.3	0.86 (< 0.011)	–	3.3

[a]Sintered α-Al_2O_3, 99.6%, Rubalit 710, Hoechst-CeramTec AG, Marktredwitz.
[b]Sapphire, (11$\bar{2}$0) single crystals, length axis = ⟨0001⟩, Kristallhandel Kelpin, Leimen.
[c]MgO, > 99.9%, (100) single crystals, length axis = ⟨100⟩, Frank and Schulte, Essen.
[d]Spinel, Kristallhandel Kelpin, Leimen.
[e]AlN, > 99.5%, sintered, SHAPAL, Parzich GmbH, Puergen.
[f]β-Si_3N_4, 95%, Frank and Schulte, Essen.
[g]α-SiC, > 98.5%, sintered + HIP, EKasid HD, Elektroschmelzwerk Kempten.
[h]β-SiC-graphite composite, ≈ 68%C, 32%Si, SiC30, Schunk, Heuchelheim.
[i]From protons. Heavy ion and neutron irradiations aim at saturation values above 0.8%.
[j]No saturation for proton doses up to 0.02 dpa in the 230°C range and up to 4 dpa at temperatures from 400 to 550°C for neutrons.
[k]No saturation for proton doses up to 0.02 dpa in the 230°C range and up to 0.1 dpa at temperatures around 600°C for neutrons.

(in units of atomic volume Ω) and for metals ranges from ≈ 2 to about 1, when the interstitials are isolated or are retained in extended sinks (e.g., dislocations), respectively. For $c_v \leq 1/v_r$ analytical solutions are possible in four different dose regimes where different types of sinks are dominating the defect inventory.

(1) At very low doses trapping of defects by preexisting lattice inhomogeneities such as dislocations and grain boundaries dominate over recombination and the atomic concentration of retained vacancies increases linearly with displacement dose Kt:

$$Kt = c_v. \tag{5}$$

(2) When loops, formed by interstitials, become the dominating sinks, one obtains

$$Kt = (\alpha c_v)^{3/2} + c_v. \tag{6}$$

The factor α depends on the ratio of the recombination rate between interstitials and vacancies to the annihilation rate of interstitials at loops and is given by $\alpha = ((2q/3Z_i)\sqrt{b/4\pi N_l})^{2/3}$.

(3) When loops entangle to form a dislocation network, the solution becomes

$$Kt = (\beta c_v)2 + c_v. \tag{7}$$

The factor β depends on the ratio of the recombination rate to the annihilation rate at dislocations and is given by: $\beta = (q/2Z_i\rho)^{1/2}$, with $\rho = \rho_d + \rho_l$ the total saturation density of dislocations.

(4) When finally recombination of interstitials with retained vacancies becomes dominating, defect production saturates:

$$c_v = 1/v_r. \tag{8}$$

This model approximately gives power law dose dependences of the relative volume change with exponents decreasing from 1 for isolated vacancies, to 2/3 for loops, to 1/2 for dislocations and finally to 0 for saturation. The transition doses between the different regimes depend on the parameters v_F, α, β and v_r. The parameters α and β contain the loop and dislocation densities which in principle can be determined from microstructural examination by transmission electron microscopy (TEM). But the onset of loop formation may be undetectable by TEM due to limited resolution. Onset of network formation is also indicated by a decrease of the lattice parameter with increasing dose, cf. the dashed line (250°C) in Fig. 1. Altogether information from microstructure is poor up to now due to lack of investigations and partially also due to limited sensitivity.

The above model was derived for monatomic materials, while ceramics are diatomic or polyatomic, i.e., at least two variants of each defect species (interstitials and vacan-

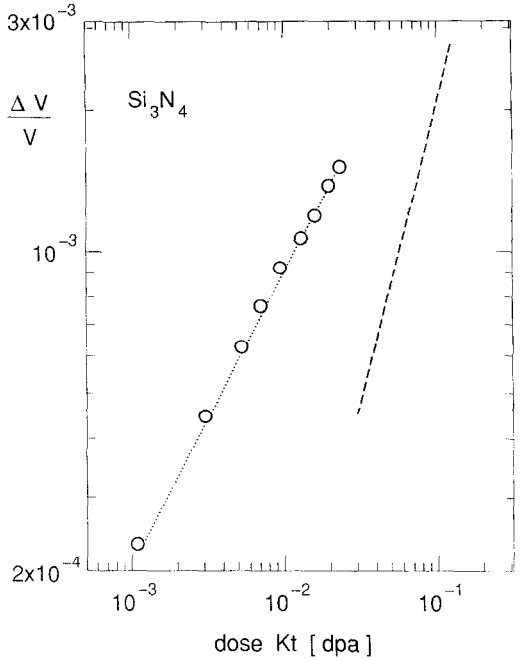

Fig. 3. Relative volume change from strains of Si_3N_4 under proton irradiation at 230°C (○) at tensile stresses of 40 MPa. A measurement at 450°C and 9 MPa gives a volume change $\leq 3\times 10^{-4}$ at 0.02 dpa. Included are results from neutron irradiations at < 660°C (- - -) [15].

cies) would have to be considered. Therefore the model is only applicable if all defects of one species show similar kinetics, being mobile or immobile, and have similar features, e.g., recombination radii, clustering strengths, etc. Only few data are available on the mobility of point defects in ceramics, which indicate that vacancies of both anions and cations are immobile up to about 330°C [20].

Results over a sufficient dose range, allowing a detailed comparison to the above model, are only available for Al_2O_3 and MgO [2]. The data were fitted by numerically solving Eqs. (1)–(3) instead of the approximate solutions, Eqs. (5)–(7). The essential fitting parameters are v_F, q, N_I and v_r, with v_F, q and N_I appearing in the intermediate dose range as a factor $v_F^3 N_I/q^2 b$ (cf. α in Eq. (6)). This means that good fits are obtained only for a constant value of this factor which amounts for Al_2O_3 to about 10^{-6}. For the low initial dislocation densities in ceramics the dislocation dominated regime is narrow and merges into the saturation regime. For a good fit in the saturation regime a constant ratio v_F/v_r must be met which roughly equals the eventual volume change $(\Delta V/V)_\infty$. For Al_2O_3 $(\Delta V/V)_\infty$ amounts to about 0.03.

There are some constraints to the parameters involved in this ratios.

(1) As already mentioned v_F of metals ranges from about 1 to 2. In ceramics there are indications that slightly higher values may occur.

(2) A lower limit of the recombination radius R_0 in q is half the interatomic distance, while an upper limit may be the radius of the recombination volume v_r. This yields for $\Omega = \langle A\rangle/\theta L_{Av} \approx 9\times 10^{-30}$ m^3 ($\langle A\rangle$ is the average atomic weight, θ is mass density and L_{Av} is Avogadro's number): 0.1 nm $\leq R_0 \leq (3v_r/4\pi)^{1/3} \approx 0.5$ nm and for q: $1\times 10^{20} \leq q \leq 5\times 10^{20}$.

(3) With these limits of q and with $1 \leq v_F \leq 5$, the

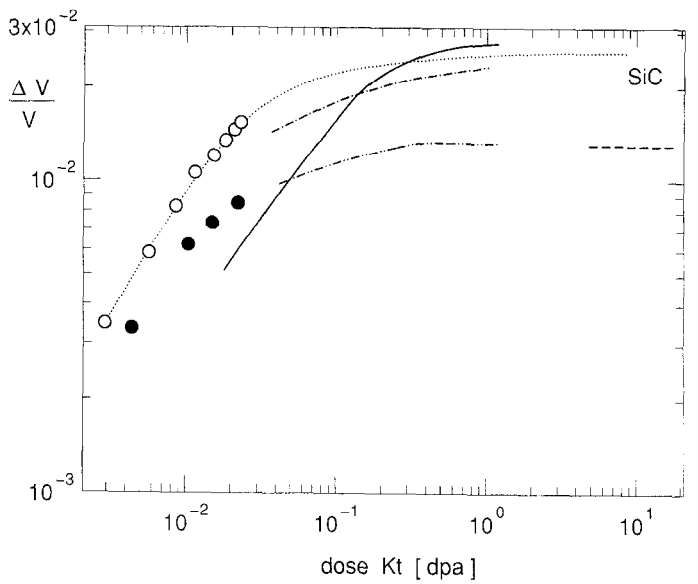

Fig. 4. Relative volume change of SiC under proton irradiation at 265°C (○) and 505°C (●). Included are results from neutron irradiations at 200°C (————) [16], 250°C (– · –), 475°C (– · · –) [17] and 500°C (- - -) [16]. The dotted line gives the results of calculations by Eq. (10).

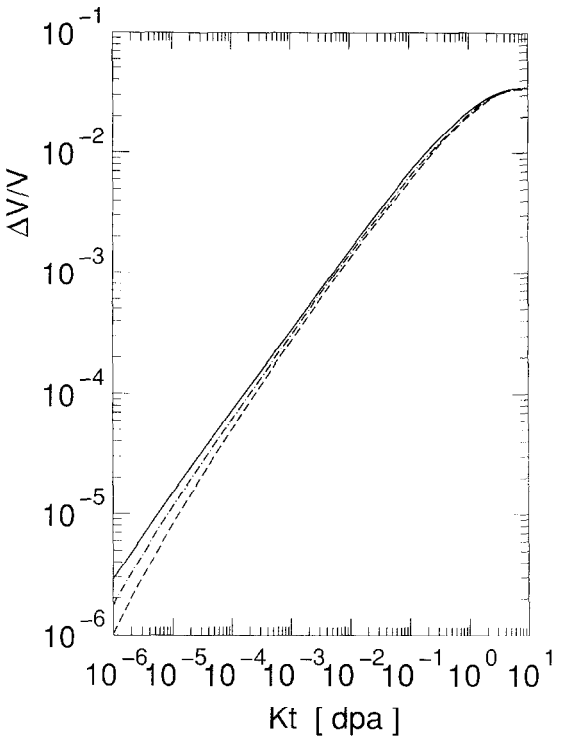

Fig. 5. Relative volume changes calculated for Al_2O_3 by numerical solution of Eqs. (1)–(3) with values for the parameters v_F, q, N_l, v_r of 1.35, 2×10^{19}, 5×10^{22}, 39 (---), 2.5, 1×10^{20}, 2×10^{23}, 75 (– · –) and 5.3, 7×10^{20}, 1×10^{24}, 166 (————), respectively. In all cases $K=2\times10^{-7}$, $D_i=3\times10^{-7}$, $b=3\times10^{-10}$, $Z_i=1.1$, $\rho_d=1\times10^{12}$ were used.

above ratio brackets the fitting values of N_l between 4×10^{22} and 1×10^{26}. Experimentally a value of $5\times10^{22}/m^3$ was observed after electron irradiation [21]. But this must be considered a lower limit, due to the limited resolution of TEM.

(4) Finally the loop radii must be significantly larger than the radius of the atomic volume.

The resulting fit for Al_2O_3 is indicated by the dotted line in Fig. 1. For example a reasonable set of parameters is $v_F\approx2.5$, $q\approx1\times10^{20}$ m^{-2}, $N_l\approx2\times10^{23}$ m^{-3} and $v_r\approx75$. Fig. 5 compares three fits with different sets of parameters, keeping $v_F^3N_l/q^2b\approx10^{-6}$ and $v_r/v_F\approx30$. Within experimental error a discrimination between the fits would only become possible if data at doses below 10^{-4} dpa would be available.

Parameter values in the same range as for Al_2O_3 are obtained by fits to the data of MgO, AlN and Si_3N_4. The two latter materials show almost constant slopes over the entire dose range, corresponding to power law exponents of ≈0.68 and ≈0.6, respectively, but no indications of saturation. Therefore v_r could not be determined. AlN shows only a minor decrease of $\Delta V/V$ from 230 to 420°C (Fig. 2), while the strains of Si_3N_4 are significantly reduced from 230 to 450°C. Due to limited resolution only an upper limit $\epsilon\le1\times10^{-4}$ can be given at 450°C for a dose of 0.02 dpa, in reasonable agreement with the neutron results at <660°C [15]. This means that in Si_3N_4 vacancies may become mobile in this temperature range.

For $MgAl_2O_4$ the situation seems more complex, with respect to volume as well as microstructural changes, cf. Ref.[2]. This may be related to a high density of structural vacancies. As indicated in Table 1, the proton data show defect saturation at much lower dose and strain levels compared to heavy ions and neutrons. It must be investigated whether there really exists a two step saturation process or if differences in the recoil spectra cause this feature.

The initial irradiation induced straining of SiC-HD (high density) as well as of a SiC-carbon composite SiC/C (30–35% graphite) is about one order of magnitude higher than for the other ceramics and shows a stronger tendency to saturation. This both facts indicate that in these materi-

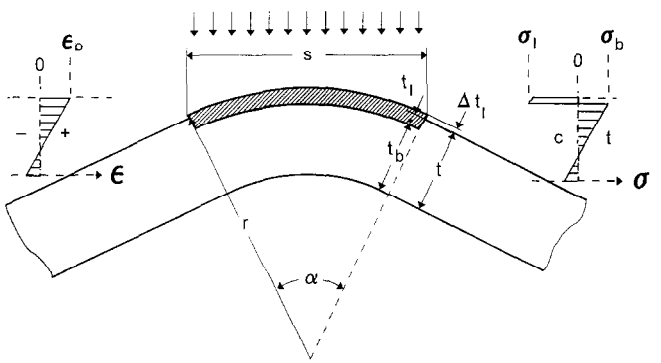

Fig. 6. Schematic views of bending of a thin bar specimen of thickness t, homogeneously implanted in a thin layer (t_l). Inserts give strain (left) and stress distribution (right), respectively.

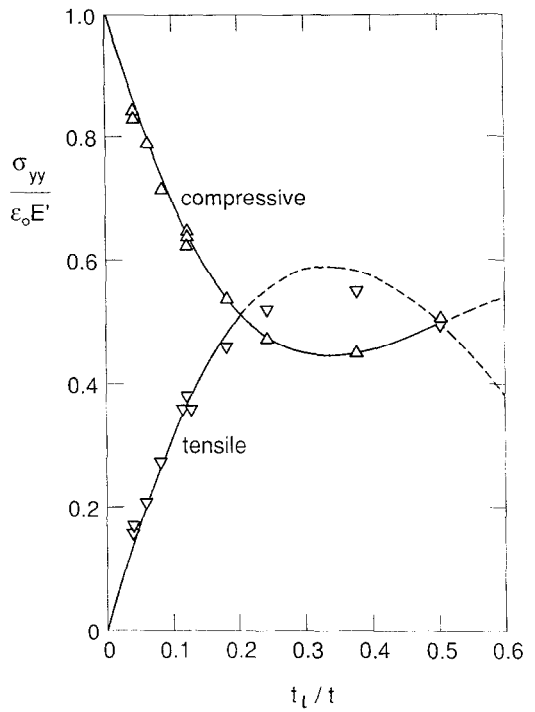

Fig. 7. Normalized lateral stresses at the interface between an irradiated/implanted layer and the bulk as a function of the ratio of layer thickness t_l to total thickness t, calculated by Eqs. (11) and (12). Symbols △ and ▽ indicate FEM calculations for the layer and matrix side, respectively.

als probably also the interstitials are immobile in the present temperature range. Therefore the rate equations for $c_i = c_v = c$ reduce to $dc/dt = K(1 - 2v_r c)$ or, if overlap of the recombination volumes is taken into account at very high c, to

$$dc/dt = K(1 - v_r c)^2, \tag{9}$$

which is solved by

$$c = Kt/(1 + Ktv_r). \tag{10}$$

This equation was fitted to the data in Fig. 4 (dotted line), giving for 265°C, $v_F \approx 1.4$ and $v_r \approx 50$.

4. Inhomogeneous irradiation / implantation

Under imhomogeneous irradiation or implantation, defect retention and the relative volume change $\Delta V/V$ due to accumulation causes internal stresses. These can approximately be described by analytical calculations. For a sketch of the geometry under consideration, i.e an irradiated layer of thickness t_l on a ribbon of total thickness t, see Fig. 6. The lateral stress at the centre of the layer/bulk interface is compressive on the layer side and is given by

$$\frac{\sigma_{yy}^{l}}{\epsilon_0 E'} \approx (1 - x)(1 - 3x + 6x^2), \tag{11}$$

with $x = t_l/t$, $\epsilon_0 = \Delta V/3V$ and $E' = E/(1 - v)$. E is the elastic modulus and v Poisson's ratio. For the matrix side (tensile stress) one obtains

$$\frac{\sigma_{yy}^{b}}{\epsilon_0 E'} \approx 4x(1 - x)^2. \tag{12}$$

Limitations of the validity of these equations can be investigated by the finite element method (FEM). Fig. 7 compares the results of FEM calculations using the pro-

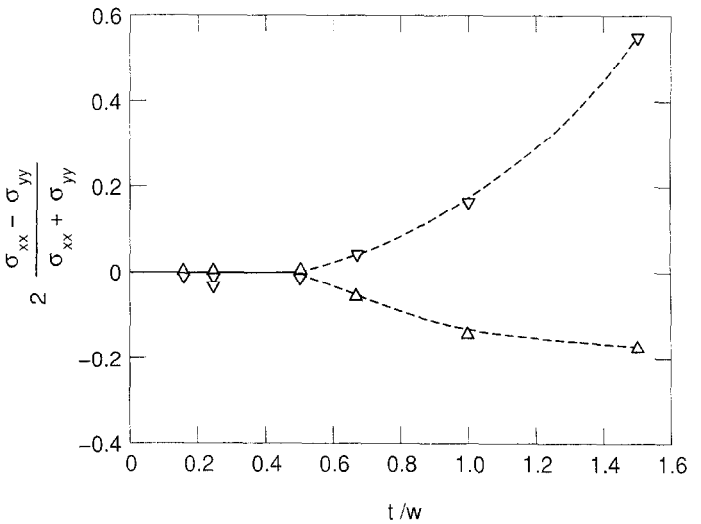

Fig. 8. Anisotropy factor of lateral stress in the centre of the irradiated area at the layer/bulk interface as a function of the thickness-to-width ratio t/w as calculated by FEM. Symbols indicate layer- (△) and bulk- (▽) side, respectively.

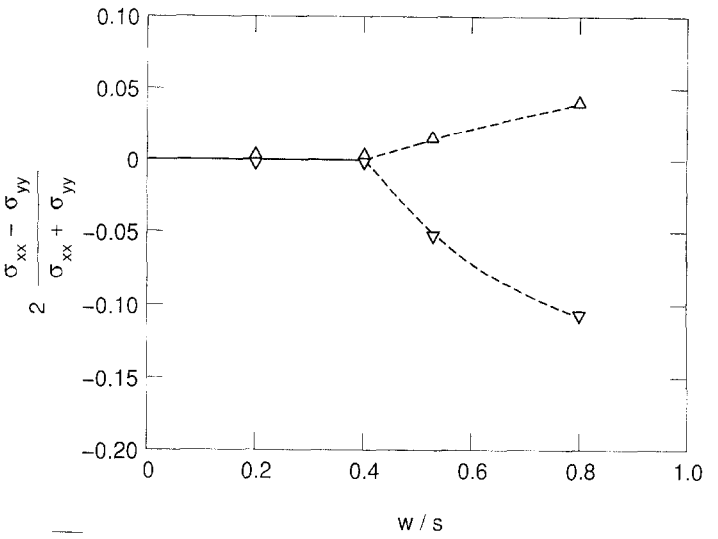

Fig. 9. Anisotropy factor of lateral stress in the centre of the irradiated area at the layer/bulk interface as a function of the ratio w/s of the width w to the length s of the irradiated area, as calculated by FEM. Symbols indicate layer- ($\triangle$) and bulk- ($\triangledown$) side, respectively.

gramme PERMAS to lines representing Eqs. (11) and (12). Eq. (11) is in reasonable agreement with the FEM calculations at least up to $x = 0.5$, while Eq. (12) deviates above $x = 0.2$. An assumption inherent to the analytical approach is the equality of the lateral stresses σ_{xx} and σ_{yy}. The FEM calculations show that even in the centre of the layer/bulk interface this assumption only holds if the lateral extension w is at least a factor of 2 larger than the thickness t (Fig. 8) and if w is smaller than the extension s of the implanted area by at least a factor of 0.4 (Fig. 9), i.e.,

$$2t \leq w \leq 0.4s. \tag{13}$$

This inequality further implies that $s \geq 5t$.

5. Bending results

In thin specimens these stresses cause bending of the irradiated part, which can be used to derive volume changes with higher sensitivity than by uniaxial length measurement. The bending radius r was determined by profilometry and strains were derived by

$$\epsilon_0 = \frac{t}{6rx(1-x)}. \tag{14}$$

Results for SiC-HD specimens of 2 mm width (w) and ≈ 0.3 mm thickness, homogeneously implanted with helium to a maximum depth of 208 μm are shown in Fig. 10. Results from uniaxial tensile straining under proton irradiation at 265°C [2,11] (see Fig. 4) are included for comparison on the basis of displacement dose. The displacement doses for the implantations was calculated by the same routine as for the above transmittent proton and neutron irradiations, cf. Table 1. Calculations by the Monte Carlo code TRIM95 [22,23] give uniformly by factors of 2 to 3 higher displacement cross section, see also Ref. [24]. Re-

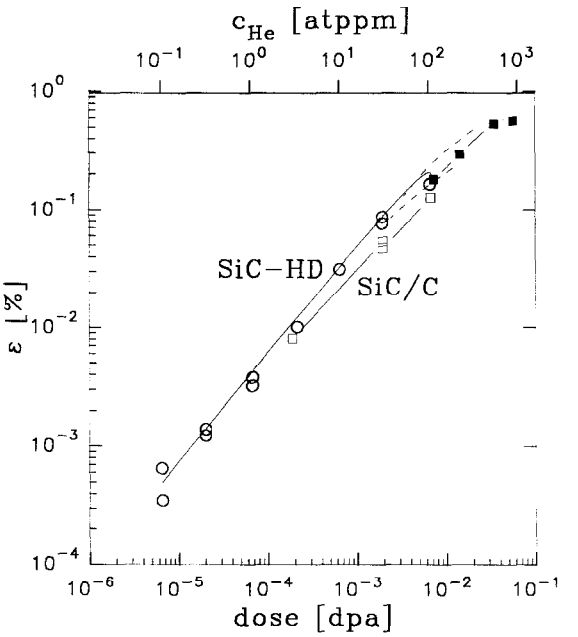

Fig. 10. Linear strains ϵ_0 derived from bending angles of 2 mm wide and 0.3 mm thick SiC-HD (○) and SiC/C (□) specimens and of 3×3 mm SiC/C specimens (■) as a function of displacement dose for helium implantation at ≤ 80°C. The upper abscissa gives the corresponding helium concentrations in the implanted region for SiC. Maximum implantation depths were 208 (○), 117 μm (□) and 244 (■), respectively. The dashed lines gives results from uniaxial tensile straining under proton irradiation of SiC at 265° [2,11] and of SiC/C at 235°C [2].

sults for SiC/C specimens with two different geometries, namely $t = w = 3$ mm and $t = 2$ mm and $w = 0.3$ mm, respectively, are included in Fig. 10. These specimens were homogeneously implanted with helium at ≤ 80°C to maximum depths of 244 and 117 μm, respectively. The helium concentrations on the upper scale correspond to the SiC-HD specimens. To conform to this scale, the SiC/C data would have to be shifted very little. The dashed lines give results from uniaxial tensile straining under proton irradiation at 265°C for SiC-HD [2,11] and 235°C for SiC/C [2], respectively.

6. Discussion and conclusions

(1) There is generally good agreement between dimensional changes induced by light ion and neutron irradiation in Al_2O_3, MgO, AlN, SiC and probably also Si_3N_4, when compared on the basis of dpa at comparable temperatures. Significant differences of saturation doses and strains between light ions and neutrons were only observed for $MgAl_2O_4$.

(2) Strains of single crystal Al_2O_3 are lower than for polycrystals at low doses but match at higher dose. This can be explained by retarded loop nucleation.

(3) The strains can be modeled by a set of rate equations for interstitials, vacancies and loops, including spontaneous recombination. But at present only a product of various parameters can be fitted.

(4) Calculations by the finite element method show that strains and stresses induced by limitation of defect production to a surface layer (implantation), can be precisely described by standard analytical equations only if the irradiation/implantation depth is less than 20% of the total thickness and if the specimen width is more than twice the thickness.

(5) This inhomogeneous irradiation causes bending by internal stress due to differential expansion. This can be used as a tool for precise strain measurements with much higher sensitivity than uniaxial length measurement or step height profilometry, cf. Ref. [25]. Strain resolutions in the ppm range are possible and are mainly limited by surface roughness. The results for SiC-HD and the SiC/C composite are in very good agreement with the uniaxial tensile measurements and can be extended to lower doses by almost three orders of magnitude. This means that application of this method to Al_2O_3 or MgO may allow to further narrow the range of fitting parameters in the rate equation model.

(6) The volume change induced by helium implantation around room temperature is essentially due to displacement defects, while the contribution of the implanted helium atoms is negligible.

Acknowledgements

The authors are indebted to I. Eppler for performing the FEM calculations and to Ms S. Hirsch for part of the Si_3N_4 irradiations.

References

[1] J. Chen, P. Jung, H. Ullmaier, Workshop on Small Scale Testing Techniques, Tougatta Onsen, Sendai, 1996, to be published.
[2] Z. Zhu, Ph.D. thesis, Report KFA Jülich, Jül-3109, Sept. 1995, ISSN 0944-2952.
[3] Z. Zhu, P. Jung, Ishino-Conference, Tokyo, 1994, to be published.
[4] D.G. Martin, J. Phys. Chem. Soc. 10 (1958) 64.
[5] J.J. Antal, A.N. Goland, Phys. Rev. 112 (1958) 105.
[6] B.S. Hickman, D.G. Walker, Proc. Br. Ceram. Soc. 7 (1967) 381.
[7] R.S. Wilks, J.A. Desport, R. Bradley, Proc. Br. Ceram. Soc. 7 (1967) 403.
[8] M. Stevanovic, J. Elston, Proc. Br. Ceram. Soc. 7 (1967) 423.
[9] R.P. Thorne, V.C. Howard, Proc. Br. Ceram. Soc. 7 (1967) 439.
[10] F.W. Clinard, J.M. Bunch, W.A. Ranken, in: Radiation Effects and Tritium Technology for Fusion Reactors, ES-ERDA CONF-750989, Vol. II, 1976, p. 498.
[11] Z. Zhu, P. Jung, J. Nucl. Mater. 212–215 (1994) 1081.
[12] T. Yano, M. Tezuka, H. Miyazaki, T. Iseki, J. Nucl. Mater. 191–194 (1992) 635.
[13] W. Dienst, J. Nucl. Mater. 191–194 (1992) 555.
[14] M. Billy, J.-C. Labbe, Y.-M. Lee, G. Roult, Rev. Int. Hautes Tempér. Refract. Fr. 21 (1984) 19.
[15] M. Billy, J.-C. Labbe, A. Selvaraj, Mater. Res. Bull. 17 (1982) 852.
[16] W. Dienst, J. Nucl. Mater. 211 (1994) 186.
[17] R.P. Thorne, V.C. Howard, B. Hope, Proc. Br. Ceram. Soc. 7 (1967) 449.
[18] E.P. Simonen, H.E. Kissinger, J.L. Brimhall, J. Nucl. Mater. 69&70 (1978) 724.
[19] V.A. Borodin, A.I. Ryazanov, D.G. Sherstennikov, J. Nucl. Mater. 202 (1993) 169.
[20] F.W. Clinard, L.W. Hobbs, in: Physics of Radiation Effects in Crystals, eds. R.A. Johnson and A.N. Orlov (North-Holland, Amsterdam, 1986) p. 387.
[21] Y. Satoh, C. Kinoshita, K. Nakai, J. Nucl. Mater. 179–181 (1991) 399.
[22] J.P. Biersack, L.G. Haggmark, Nucl. Instrum. Meth. 174 (1980) 93.
[23] J.F. Ziegler, Manual TRIM Version 95.4, Mar. 1995, unpublished.
[24] Z. Zhu, P. Jung, Nucl. Instrum. Meth. B91 (1994) 269.
[25] G.P. Pells, M.J. Murphy, J. Nucl. Mater. 183 (1991) 137.